# Critical temperature $T_c$ and memory kernel in molecular-dynamics-simulated glass-forming $Ni_{0.2}Zr_{0.8}$

A. B. Mutiara* and H. Teichler†

*Institut für Materialphysik, Universität Göttingen, Hospitalstrasse 3-7, D-37073 Göttingen, Germany*
(Received 20 July 2000; revised manuscript received 7 June 2001; published 26 September 2001)

The mode-coupling theory (MCT) of dense liquids marks the dynamical glass transition by a critical temperature $T_c$ that is reflected in the temperature dependence of a number of physical quantities. Here, molecular-dynamics simulation data of a model adapted to $Ni_{0.2}Zr_{0.8}$ are analyzed to deduce $T_c$ from different quantities and to check the consistency of the estimated values. Analyzed are the critical temperature $T_c$ from (i) the nonvanishing nonergodicity parameters as asymptotic solutions of the MCT equations in the arrested state, (ii) the $\mathbf{g}_m$ parameters describing the approach of the melt towards the arrested state on the ergodic side, (iii) the diffusion coefficients in the melt, and (iv) the $\alpha$-relaxation time. The resulting $T_c$ values are found to agree within about 10%. In addition, the time dependent memory kernel is calculated from the MCT for the incoherent intermediate scattering function around $T_c$ and compared with the kernel obtained by inverting the molecular dynamics data for the corresponding correlator.

## I. INTRODUCTION

At present the phenomena behind the liquid-glass transition and the nature of the glassy state are not fully understood, despite the progresses of recent years. In contrast to usual phase transformations the glass transition seems to be primarily dynamical in origin [1,2] and therefore new theoretical approaches have to be developed for its description. Several theoretical models have been proposed to explain the transition and the corresponding experimental data. The latter concern both *the temperature dependence of particular properties*, such as the shear viscosity and the structural relaxation time, and *the time dependent response* as visible in the dielectric susceptibility, inelastic neutron scattering, and light scattering spectra investigations. The spectral measurements have been extended to cover the large frequency range from below the primary $\alpha$-relaxation peak up to the high-frequency region of microscopic dynamics dominated by vibrational modes [3,4].

One of the promising theoretical approaches in this field is the mode-coupling theory (MCT). The MCT originally was developed to model critical phenomena [5,6]. The non-classical behavior of the transport properties near the critical point was thought to be caused by nonlinear couplings between slow (hydrodynamic and order parameter) modes of the system. In later years, the MCT was found to be applicable more generally to describe nonlinear effects in dense liquids [7] and nonhydrodynamic effects in the case of the glass transition.

In its simplest (''idealized'') version, first analyzed in the ''schematic'' approach by Bengtzelius *et al.* [8] and independently by Leutheusser [9], the MCT predicts a transition from a high temperature liquid (''ergodic'') state to a low temperature arrested (''nonergodic'') state at a critical tem-

perature $T_c$. Including transverse currents as additional hydrodynamic variables, the full MCT shows no longer a sharp transition at $T_c$ but all structural correlations decay in a final $\alpha$ process [2]. Similar effects are expected from inclusion of thermally activated matter transport, that means, diffusion in the arrested state [10,11].

In the full MCT, the remainders of the transition and the value of $T_c$ have to be evaluated, e.g., from the approach of the undercooled melt towards the idealized arrested state, either by analyzing the time and temperature dependence in the $\beta$ regime of the structural fluctuation dynamics [12–14] or by evaluating the temperature dependence of the so-called $\mathbf{g}_m$ parameter [15,16]. There are further possible ways to estimate $T_c$, e.g., from the temperature dependence of the diffusion coefficients or the relaxation time of the final $\alpha$ decay in the melt, as these quantities for $T > T_c$ display a critical behavior $|T - T_c|^{\pm \gamma}$. However, only crude estimates of $T_c$ can be obtained from these quantities, since near $T_c$ the critical behavior is masked by the effects of transverse currents and thermally activated matter transport, as mentioned above.

On the other hand, as emphasized and applied in [17–19], the value of $T_c$ predicted by the idealized MCT can be calculated once the partial structure factors of the system and their temperature dependence are sufficiently well known. Besides temperature and particle concentration, the partial structure factors are the only significant quantities that enter the equations of the so-called nonergodicity parameters of the system. The latter vanish identically for temperatures above $T_c$ and their calculation thus allows a rather precise determination of the critical temperature predicted by the idealized theory.

At this stage it is tempting to consider how well the estimates of $T_c$ from different approaches fit together and whether the $T_c$ estimate from the nonergodicity parameters of the idealized MCT compares to the values from the full MCT. Regarding this, we here investigate a molecular dynamics (MD) simulation model adapted to the glass-forming

*Permanent address: Gunadarma University, Jln. Margonda Raya 100, Pondok–Cina Depok, Indonesia.

†Email address: teichler@umpa06.gwdg.de

$Ni_{0.2}Zr_{0.8}$ transition metal system. The $Ni_xZr_{1-x}$ system is well studied by experiments [20,21] and by MD simulations [22–30], as it is a rather interesting system whose components are important constituents of a number of multicomponent ''massive'' metallic glasses. In the present contribution we consider, in particular, the $x=0.2$ composition and concentrate on the determination of $T_c$ from evaluating and analyzing the nonergodicity parameter, the $\mathbf{g}_m(T)$ parameter in the ergodic regime, the diffusion coefficients, and the $\alpha$-decay relaxation time.

In the literature, similar comparison of $T_c$ estimates already exist [17–19] for two systems. The studies come, however, to rather different conclusions. From MD simulations for a soft spheres model, Barrat and Latz [17] find an agreement between the different $T_c$ estimates within about 15%. On the other hand, for a binary Lennard-Jones system, Nauroth and Kob [19] get from their MD simulations a significant deviation between the $T_c$ estimates by about a factor of 2. Regarding this, the present investigation is aimed at clarifying the situation for at least one of the important metallic glass systems.

Our paper is organized as follows: In Sec. II, we present the model and give some details of the computations. Section III gives a brief discussion of some aspects of the mode-coupling theory as used here. Results of our MD simulations and their analysis are then presented and discussed in Sec. IV.

## II. SIMULATIONS

The present simulations are carried out as state-of-the-art isothermal-isobaric $(N,T,p)$ calculations. The Newtonian equations of $N=648$ atoms (130 Ni and 518 Zr) are numerically integrated by a fifth order predictor-corrector algorithm with time step $\Delta t = 2.5 \times 10^{-15}$ s in a cubic volume with periodic boundary conditions and variable box length $L$. With regard to the electron theoretical description of the interatomic potentials in transition metal alloys by Hausleitner and Hafner [31], we model the interatomic couplings as in [23] by a volume dependent electron-gas term $E_{vol}(V)$ and pair potentials $\phi(r)$ adapted to the equilibrium distance, depth, width, and zero of the Hausleitner-Hafner potentials [31] for $Ni_{0.2}Zr_{0.8}$ [32]. For this model, simulations were started through heating a starting configuration up to 2000 K that leads to a homogeneous liquid state. The system then is cooled continuously to various annealing temperatures with cooling rate $-\partial_t T = 1.5 \times 10^{12}$ K/s. Afterwards the obtained configurations at various annealing temperatures (here 1500–800 K) are relaxed by carrying out additional isothermal annealing runs. Finally the time evolution of these relaxed configurations is modeled and analyzed. More details of the simulations are given in Ref. [32].

## III. THEORY

### A. Nonergodicity parameters

In this section we provide some basic formulas that permit calculation of $T_c$ and the nonergodicity parameters $f_{ij}(q)$ for our system. A more detailed presentation may be found

in Refs. [17,33,34,18,19]. The central object of the MCT are the partial intermediate scattering functions that are defined for a binary system by [35]

$$F_{ij}(q,t) = \frac{1}{\sqrt{N_i N_j}} \langle \rho^i(q,t)\rho^j(-q,0) \rangle$$

$$= \frac{1}{\sqrt{N_i N_j}} \sum_{\alpha=1}^{N_i} \sum_{\beta=1}^{N_j} \times \langle \exp\{i\mathbf{q}\cdot[\mathbf{r}_\alpha^i(t)-\mathbf{r}_\beta^j(0)]\} \rangle,$$

$$(1)$$

where

$$\rho(\mathbf{q}) = \sum_{\alpha=1}^{N_i} e^{i\mathbf{q}\cdot\mathbf{r}_{\alpha i}}, \quad i=1,2 \tag{2}$$

is a Fourier component of the microscopic density of species $i$.

The diagonal terms $\alpha=\beta$ are denoted as the incoherent intermediate scattering function

$$F_i^s(q,t) = \frac{1}{N_i} \sum_{\alpha=1}^{N_i} \langle \exp\{i\mathbf{q}\cdot[\mathbf{r}_\alpha^i(t)-\mathbf{r}_\alpha^i(0)]\} \rangle. \tag{3}$$

The normalized partial and incoherent intermediate scattering functions are given by

$$\Phi_{ij}(q,t) = F_{ij}(q,t)/S_{ij}(q), \tag{4}$$

$$\Phi_i^s(q,t) = F_i^s(q,t), \tag{5}$$

where the $S_{ij}(q) = F_{ij}(q,t=0)$ are the partial static structure factors.

The basic equations of the MCT are the set of nonlinear matrix integro-differential equations

$$\ddot{\mathbf{F}}(q,t) + \mathbf{\Omega}^2(q)\mathbf{F}(q,t) + \int_0^t d\tau \mathbf{M}(q,t-\tau)\dot{\mathbf{F}}(q,\tau) = 0, \tag{6}$$

where $\mathbf{F}$ is the $2\times2$ matrix consisting of the partial intermediate scattering functions $F_{ij}(q,t)$, and the frequency matrix $\mathbf{\Omega}^2$ is given by

$$[\mathbf{\Omega}^2(q)]_{ij} = q^2 k_B T(x_i/m_i) \sum_k \delta_{ik}[\mathbf{S}^{-1}(q)]_{kj}. \tag{7}$$

$\mathbf{S}(q)$ denotes the $2\times2$ matrix of the partial structure factors $S_{ij}(q)$, $x_i = N_i/N$, and $m_i$ means the atomic mass of the species $i$. The MCT for the idealized glass transition predicts [2] that the memory kernel $\mathbf{M}$ can be expressed at long times by

$$M_{ij}(\mathbf{q},t) = \frac{k_B T}{2\rho m_i x_j} \int \frac{d\mathbf{k}}{(2\pi)^3} \sum_{kl} \sum_{k'l'} V_{ikl}(\mathbf{q},\mathbf{k}) V_{jk'l'}(\mathbf{q},\mathbf{q}-\mathbf{k})$$

$$\times F_{kk'}(\mathbf{k},t)F_{ll'}(\mathbf{q}-\mathbf{k},t), \tag{8}$$

where $\rho = N/V$ is the particle density and the vertex $V_{i\alpha\beta}(\mathbf{q},\mathbf{k})$ is given by

$$V_{ikl}(\mathbf{q},\mathbf{k}) = \frac{\mathbf{q}\cdot\mathbf{k}}{q}\delta_{il}c_{ik}(\mathbf{k}) + \frac{\mathbf{q}\cdot(\mathbf{q}-\mathbf{k})}{q}\delta_{ik}c_{il}(\mathbf{q}-\mathbf{k}) \quad (9)$$

and the matrix of the direct correlation function is defined by

$$c_{ij}(\mathbf{q}) = \frac{\delta_{ij}}{x_i} - [\mathbf{S}^{-1}(\mathbf{q})]_{ij}. \quad (10)$$

The equation of motion for $F_i^s(q,t)$ has a similar form as Eq. (6), but the memory function for the incoherent intermediate scattering function is given by

$$M_i^s(\mathbf{q},t) = \int \frac{d\mathbf{k}}{(2\pi)^3}\frac{1}{\rho}\left(\frac{\mathbf{q}\cdot\mathbf{k}}{q}\right)(cF)_i(\mathbf{k},t)F_i^s(\mathbf{q}-\mathbf{k},t), \quad (11)$$

$$(cF)_i(k,t) = [c_{ii}(q)]^2 F_{ii}(q,t) + 2c_{ii}(q)c_{ij}(q)F_{ij}(q,t) + [c_{ij}(q)]^2 F_{jj}(q,t) \quad j\neq i. \quad (12)$$

In order to characterize the long time behavior of the intermediate scattering function, the nonergodicity parameters $\mathbf{f}(\mathbf{q})$ are introduced as

$$f_{ij}(\mathbf{q}) = \lim_{t\to\infty}\Phi_{ij}(\mathbf{q},t). \quad (13)$$

These parameters are the solution of Eqs. (6)–(10) at long times. The meaning of these parameters is the following: if $f_{ij}(\mathbf{q}) = 0$, then the system is in a liquid state with density fluctuation correlations decaying at long times. If $f_{ij}(\mathbf{q}) > 0$, the system is in an arrested, nonergodic state, where density fluctuation correlations are stable for all times. In order to compute $f_{ij}(\mathbf{q})$, one can use the following iterative procedure [19]:

$$\mathbf{f}^{(l+1)}(q) = \frac{\mathbf{S}(q)\cdot\mathbf{N}[\mathbf{f}^{(l)},\mathbf{f}^{(l)}](q)\cdot\mathbf{S}(q)}{Z}$$
$$+ \frac{q^{-2}|\mathbf{S}(q)||\mathbf{N}[\mathbf{f}^{(l)},\mathbf{f}^{(l)}](q)|\mathbf{S}(q)}{Z}, \quad (14)$$

$$Z = q^2 + \mathrm{Tr}(\mathbf{S}(q)\cdot\mathbf{N}[\mathbf{f}^{(l)},\mathbf{f}^{(l)}](q))$$
$$+ q^{-2}|\mathbf{S}(q)||\mathbf{N}[\mathbf{f}^{(l)},\mathbf{f}^{(l)}](q)|,$$

where the matrix $\mathbf{N}(q)$ is given by

$$N_{ij}(q) = \frac{m_i}{x_i k_B T}M_{ij}(q). \quad (15)$$

This iterative procedure, indeed, has two types of solutions, nontrivial ones with $\mathbf{f}(q) > 0$ and trivial solutions $\mathbf{f}(q) = 0$.

The incoherent nonergodicity parameter $f_i^s(q)$ can be evaluated by the following iterative procedure:

$$q^2\frac{f_i^{s,l+1}(q)}{1-f_i^{s,l+1}(q)} = M_i^s[\mathbf{f},f_i^{s,l}](q). \quad (16)$$

As indicated by Eq. (16), computation of the incoherent nonergodicity parameter $f_i^s(q)$ demands that the coherent nonergodicity parameters are determined in advance.

### B. $\mathbf{g}_m$ parameter

Beyond the details of the MCT, equations of motion like Eq. (6) can be derived for the correlation functions under rather general assumptions within the Lanczos recursion scheme [38] resp. the Mori-Zwanzig formalism [39]. The approach demands that the time dependence of fluctuations A, B, ... is governed by a time evolution operator like the Liouvillian and that for two fluctuating quantitites a scalar product (B, A) with the meaning of a correlation function can be defined. In case of a tagged particle, this leads for $\Phi_i^s(q,t)$ to the exact equation

$$\ddot{\Phi}_i^s(q,t)/\Omega_0^2 + \Phi_i^s(q,t) + \int_0^t d\tau M_i^0(q,t-\tau)\dot{\Phi}_i^s(q,\tau) = 0 \quad (17)$$

with memory kernel $M_i^0(q,t)$ in terms of a continued fraction.

Within $M_i^0(q,t)$ are hidden all the details of the time evolution of $\Phi_i^s(q,t)$. As proposed and applied in Refs. [15,16], instead of calculating $M_i^0(q,t)$ from the time evolution operator as a continued fraction, it can be evaluated in closed forms once $\Phi_i^s(q,t)$ is known, e.g., from experiments or MD simulations. This can be demonstrated by introduction of

$$\Phi_c(\omega)\pm i\Phi_s(\omega) := \lim_{\varepsilon\to 0}\mathcal{L}\{\Phi\}(\varepsilon\mp i\omega), \quad (18)$$

with

$$\mathcal{L}\{\Phi\}(z) = \int_0^\infty dt\, e^{-zt}\Phi(t) \quad (19)$$

the Laplace transform of $\Phi(t)$, and

$$M_i^0(\omega)_c\pm iM_i^0(\omega)_s := \lim_{\varepsilon\to 0}\mathcal{L}\{M_i^0\}(\varepsilon\mp i\omega). \quad (20)$$

Equation (17) then leads to

$$M_i^0(\omega)_c = \frac{\Phi_c(\omega)}{[1-\omega\Phi_s(\omega)]^2 + [\omega\Phi_c(\omega)]^2}. \quad (21)$$

On the time axis, $M_i^0(t)$ is given by

$$M_i^0(t) = \frac{2}{\pi}\int_0^\infty d\omega M_i^0(\omega)_c\cos(\omega t). \quad (22)$$

Equation (17) leads to an arrested state, that means to an asymptotically finite correlation $\Phi_i^s(q,t\to\infty) > 0$, if $M_i^0(q,t\to\infty)$ remains finite where the relationship has to hold

$$M_i^0(q,t\to\infty)[\Phi_i^s(q,t\to\infty)^{-1}-1] = 1. \quad (23)$$

In order to characterize the undercooled melt and its transition into the glassy state, we introduced in Ref. [15] the function

$$\mathbf{G}(\Phi, M^0) := M^0(t)[\Phi(t)^{-1} - 1]. \tag{24}$$

According to Eq. (23), $\mathbf{G}(\Phi, M^0)$ has the property that

$$\mathbf{G}(\Phi, M^0)|_{t \to \infty} = 1 \tag{25}$$

in the arrested, nonergodic state. On the other hand, if

$$\mathbf{g}_m := \max\{\mathbf{G}(\Phi, M^0) | 0 < t < \infty\} < 1, \tag{26}$$

there is no arrested solution and the correlations $\Phi_i^s(q,t)$ decay to zero for $t \to \infty$, that means, the system is in the liquid state. From that we proposed [15] to use the value of $\mathbf{g}_m$ as a relative measure of the extent to which the system has approached the arrested state and to use the temperature dependence of $\mathbf{g}_m(T)$ in the liquid state as an indication of how the system approaches this state.

## IV. RESULTS AND DISCUSSIONS

### A. Partial structure factors and intermediate scattering functions

First we show the results of our simulations concerning the static properties of the system in terms of the partial structure factors $S_{ij}(q)$ and partial correlation functions $g_{ij}(r)$.

To compute the partial structure factors $S_{ij}(q)$ for a binary system we use the following definition [40]:

$$S_{ij}(\mathbf{q}) = x_i \delta_{ij} + \rho x_i x_j \int [g_{ij}(\mathbf{r}) - 1] e^{-i\mathbf{q}\cdot\mathbf{r}} d\mathbf{r}, \tag{27}$$

where

$$g_{ij}(\mathbf{r}) = \frac{V}{N_i N_j} \left\langle \sum_{\alpha=1}^{N_i} \sum_{\beta=1, \beta \neq \alpha}^{N_j} \delta(\mathbf{r} - [\mathbf{r}_\alpha(t) - \mathbf{r}_\beta(t)]) \right\rangle \tag{28}$$

are the partial pair correlation functions.

The MD simulations yield a periodic repetition of the atomic distributions with periodicity length $L$. Truncation of the Fourier integral in Eq. (27) leads to an oscillatory behavior of the partial structure factors at small $q$. In order to reduce the effects of this truncation, we compute from Eq. (28) the partial pair correlation functions for distance $r$ up to $R_c = 3/2L$. For numerical evaluation of Eq. (27), a Gaussian-type damping term is included,

$$S_{ij}(q) = x_i \delta_{ij} + 4\pi\rho x_i x_j \int_0^{R_c} r^2 [g_{ij}(r) - 1] \frac{\sin(qr)}{qr}$$

$$\times \exp[-(r/R)^2] dr \tag{29}$$

with $R = R_c/3$.

Figure 1 shows the partial structure factors $S_{ij}(q)$ versus $q$ for all temperatures investigated. The figure indicates that the shape of $S_{ij}(q)$ depends only weakly on temperature and
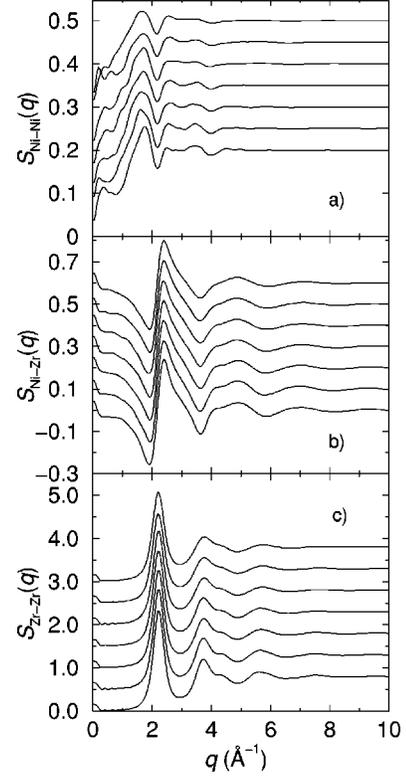


FIG. 1. Partial structure factors at $T = 1400$, 1300, 1200, 1100, 1000, 900, and 800 K (from top to bottom); (a) Ni-Ni part (the curves are vertically shifted by 0.05 relative to each other); (b) Ni-Zr part (the curves are vertically shifted by 0.1 relative to each other); and (c) Zr-Zr part (the curves are vertically shifted by 0.5 relative to each other).

that the positions of the first maximum and the first minimum are more or less temperature independent, as also found, e.g., for the $A_{0.8}B_{0.2}$ Lennard-Jones model [41].

In order to compare our calculated structure factors with experimental ones, we have determined the Faber-Ziman partial structure factors $a_{ij}(q)$ [43]

$$a_{ij}(\mathbf{q}) = 1 + \rho \int (g_{ij} - 1) e^{-i\mathbf{q}\cdot\mathbf{r}} d\mathbf{r}, \tag{30}$$

and the Faber-Ziman total structure factor $S_{tot}^{FZ}(q)$ [42]. For a binary system with coherent scattering length $b_i$ of species $i$ the following relationship holds:

$$S_{tot}^{FZ}(q) = \frac{1}{\langle b \rangle^2} [x_1^2 b_1^2 a_{11}(q) + x_2^2 b_2^2 a_{22}(q)$$

$$+ 2x_1 x_2 b_1 b_2 a_{12}(q)]. \tag{31}$$

In the evaluation of $a_{ij}(q)$, we applied the same algorithm as for $S_{ij}(q)$. By using $a_{ij}(q)$ and with aids of the experimental data of the average scattering length $b$ one can compute the total structure factor. Here we take $b_i$ from the experimental data of Kuschke [20]. For natural Ni $b = 1.03 \times 10^{-12}$ cm and for Zr $b = 0.716 \times 10^{-12}$ cm. Figure 2 compares the results of our simulations with the experimental
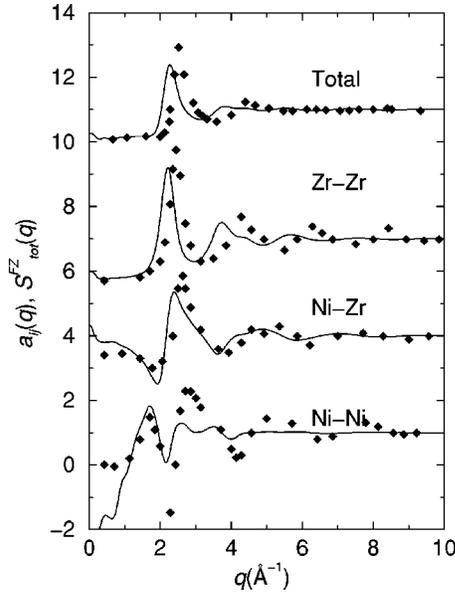
FIG. 2. Comparison between our MD simulations and experimental results [20] of the total Faber-Ziman structure factor $S_{tot}^{FZ}(q)$ and the partial Faber-Ziman structure factors $a_{ij}(q)$ for $Ni_{0.2}Zr_{0.8}$.

results by Kuschke [20] for the same alloy system at 1000 K. There is a good agreement between the experimental and the simulation data which demonstrates that our model is able to reproduce the steric relations of the considered system and the chemical order, as far is visible in the partial structure factors.

To investigate the dynamical properties of the system, we have calculated the incoherent scattering function $F_i^s(q,t)$ and the coherent scattering function $F_{ij}(q,t)$ as defined in equations (1) and (3). Figure 3 presents the normalized co-
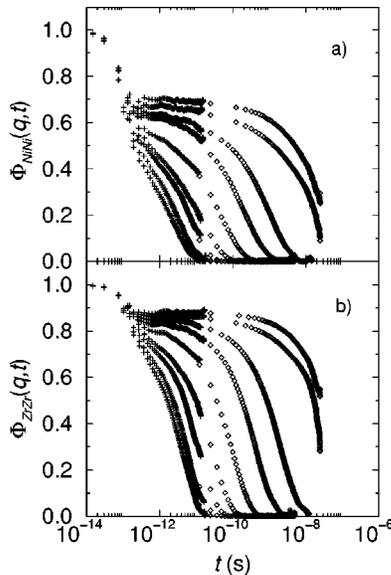


FIG. 3. Coherent intermediate scattering function $\Phi_{ii}(q,t)$ for $q=21.6$ nm$^{-1}$ at $T=1500, 1400, 1300, 1200, 1100, 1000, 950, 900,$ and 800 K (from left to right); (a) Ni-Ni part and (b) Zr-Zr part.

herent intermediate scattering functions $\Phi_{ii}(q,t)$ of both species evaluated from our MD data for wave vector $q_n = 2\pi n/L$ with $n=9$, that means $q_9 = 21.6$ nm$^{-1}$. The incoherent intermediate scattering functions display a rather similar behavior. From the figure we see that the $\Phi_{ii}(q,t)$ of both species show at intermediate temperatures a structural relaxation in three succesive steps as predicted by the idealized schematic MCT [44]. The first step is a fast initial decay on the time scale of the vibrations of atoms ($t<0.2$ ps). This step is characterized by the MCT only globally. The second step is the $\beta$-relaxation regime. In the early $\beta$ regime the correlator should decrease according to $\Phi_{ii}(q,t)=f_{cii}(q) + A/t^a$ and in the late $\beta$-relaxation regime, which appears only in the melt, according the von Schweidler law $\Phi_{ii}(q,t)=f_{cii}(q)-Bt^b$. Between them a wide plateau is found near the critical temperature $T_c$. In the melt, the $\alpha$ relaxation takes place as the last decay step after the von Schweidler law. It can be described by the Kohlrausch-Williams-Watts (KWW) law $\Phi_{ii}(q,t)=A_0 \exp[-(t/\tau_\alpha)^\beta]$, where the relaxation time $\tau_\alpha$ near the glass transition shifts drastically to longer times.

The inverse power-law decay for the early $\beta$ regime $\Phi \sim f_c + A/t^a$ is not seen in our data. This seems to be due to the fact that in our system the power-law decay is dressed by the atomic vibrations ( [15,16] and references therein).

According to our MD results, $\Phi_{ii}(q,t)$ decays to zero for longer times at all temperatures investigated. This is in agreement with the full MCT. Including transversal currents as additional hydrodynamic variables, the full MCT [2] comes to the conclusion that all structural correlations decay in the final $\alpha$ process, independent of temperature. Similar effects are expected from inclusion of thermally activated matter transport, that means diffusion in the arrested state.

At $T=800$ K and 900 K, the $\Phi_{ii}(q,t)$ drop rather sharply at large $t$. This reflects aging effects that take place if a system is in a transient, nonsteady state [45]. Such a behavior indicates relaxations of the system on the time scale of the ''measuring time'' of the correlations.

### B. Nonergodicity parameters

The nonergodicity parameters are defined by Eq. (13) as a nonvanishing asymptotic solution of the MCT Eq. (6). Phenomenologically, they can be estimated by creating a master curve from the intermediate scattering functions with fixed scattering vector $q$ at different temperatures. The master curves are obtained by plotting the scattering functions $\Phi(q,t)$ as function of the normalized time $t/\tau_\alpha$. As an example, Fig. 4 presents the master curves for $q=21.6$ nm$^{-1}$ constructed from the coherent scattering functions of Fig. 3. In the asymptotic regime, the master curves can be approximated by the KWW law $\Phi(q,t)=A(q)\exp[-(t/\tau_\alpha)^{-\beta}]$, in the late $\beta$ regime by the von Schweidler law $\Phi(q,t) = f_c(q)-B(t/\tau_\alpha)^b$. The so-constructed $f_c(q)$ should agree with the nonergodicity parameter. In our case, both laws are good approximations of the master curves as demonstrated by Fig. 4. Figure 5 presents the estimated $q$-dependent nonergodicity parameters from the coherent scattering functions of Ni and Zr, Fig. 6 presents those from the incoherent
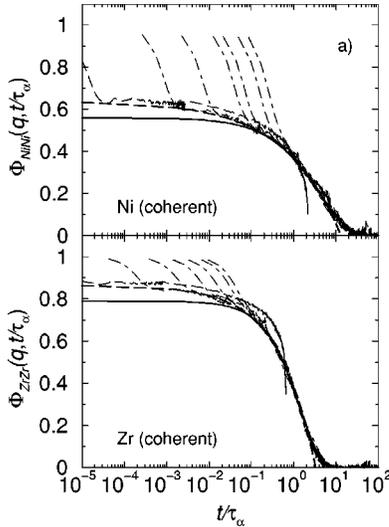
FIG. 4. Master curve for the coherent intermediate scattering function constructed from the $T=900$, 1000, 1100, 1200, 1300, 1400, and 1500 K data (dash-dotted line from left to right): (a) Ni-Ni part and (b) Zr-Zr part. The bold dashed line is a fit with the von Schweidler law; the bold solid line is a fit with KWW law.

scattering functions. In Figs. 5 and 6 are also included the deduced KWW amplitudes $A(q)$ from the master curves and from the intermediate scattering functions at $T=1100$ K. (The further fit parameters can be found in [32].)

In order to compute the nonergodicity parameters $f_{ij}(q)$ analytically, we followed for our binary system the self-consistent method as formulated by Nauroth and Kob [19] and as sketched in Sec. III A. Input data for our iterative determination of $f_{ij}(q)=F_{ij}(q,\infty)$ are the temperature de-
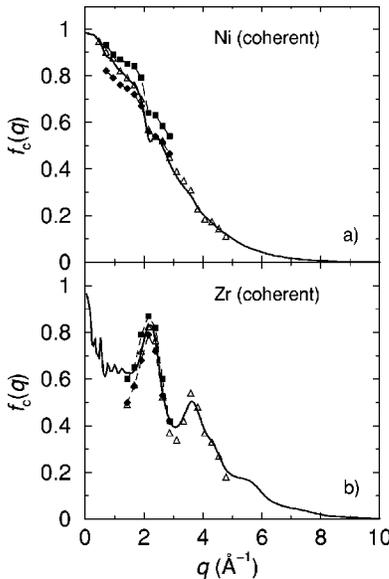


FIG. 5. Nonergodicity parameter $f_{cij}$ for the coherent interme-diate scattering functions as solutions of Eqs. (7) and (8) (solid line), KWW parameter $A(q)$ of the master curves (diamond), von Schweidler parameter $f_c(q)$ of the master curves (square), and KWW parameter $A(q)$ for $\Phi_{ij}(q)$ at 1100 K (triangle up); (a) Ni-Ni part and (b) Zr-Zr part.
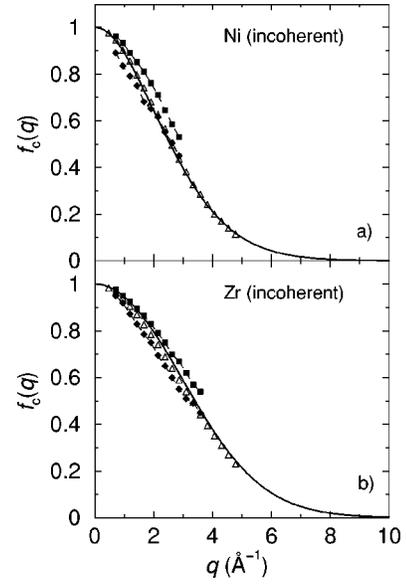


FIG. 6. The same as Fig. 5 but for the incoherent intermediate scattering function; (a) Ni part and (b) Zr part.

pendent partial structure factors $S_{ij}(q)$ from the previous subsection. The iteration is started by arbitrarily setting $F_{Ni\text{-}Ni}(q,\infty)^{(0)}=0.5S_{Ni\text{-}Ni}(q)$, $F_{Zr\text{-}Zr}(q,\infty)^{(0)}=0.5S_{Zr\text{-}Zr}(q)$, $F_{Ni\text{-}Zr}(q,\infty)^{(0)}=0$.

For $T>1200$ K we always obtain the trivial solution $f_{ij}(q)=0$ while at $T=1100$ K and below we get stable non-vanishing $f_{ij}(q)>0$. The stability of the nonvanishing solu-tions was tested for more than 3000 iteration steps. From these results we expect that $T_c$ for our system lies between 1100 and 1200 K. To estimate $T_c$ more precisely, we inter-polated $S_{ij}(q)$ from our MD data for temperatures between 1100 and 1200 K by use of the algorithm of Press *et al.* [46]. We observe that at $T=1102$ K a nontrivial solution of $f_{ij}(q)$ can be found, but not at $T=1105$ K and above. It means that the critical temperature $T_c$ for our system is around 1102 K. The nontrivial solutions $f_{ij}(q)$ for this tem-perature shall be denoted the critical nonergodicty param-eters $f_{cij}(q)$. They are included in Fig. 5. As can be seen from Fig. 5, the absolute values and the $q$ dependence of the calculated $f_{cij}(q)$ agree rather well with the estimates from the scattering functions master curve and, in particular, with the deduced KWW amplitudes $A(q)$ at 1100 K.

By use of the critical nonergodicity parameters $f_{cij}(q)$, the computational procedure was run to determine the criti-cal nonergodicity parameters $f_{ci}^s(q)$ for the incoherent scat-tering functions at $T=1102$ K. Figure 6 presents our results for the so-calculated $f_{ci}^s(q)$. Like Fig. 5 for the coherent nonergodicity parameters, Fig. 6 demonstrates for the $f_{ci}^s(q)$ that they agree well with the estimates from the incoherent scattering functions master curve and, in particular, with the deduced KWW amplitudes $A(q)$ at 1100 K.

Regarding the good agreement between the nonergodicity parameters and KWW amplitudes, our results reconfirm the corresponding observation by Nauroth and Kob [19] in their Lennard-Jones simulations. There is, however, a fundamen-
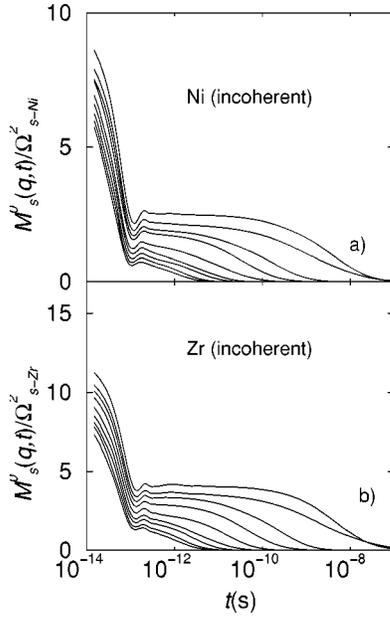
FIG. 7. Time dependence of the dimensionless memory function $M_s^0(q,t)/\Omega_{s-i}^2$ from MD simulations for $q_9 = 21.6$ nm$^{-1}$ and $T = 800, 900, 950, 1000, 1100, 1200, 1300, 1400,$ and $1500$ K (from top to bottom); (a) Ni part and (b) Zr part.

tal difference between our results and the Lennard-Jones calculations concerning the value of $T_c$. The $T_c$ value of 1102 K determined for the present model from the nonergodicity parameters agrees within 10–15 % with the $T_c$ values from other estimates, as we shall demonstrate in the following sections, while a deviation by a factor of 2 was found in the Lennard-Jones modeling [19].

### C. $\mathbf{g}(\Phi_i^s, M_i^0)$ function and $\mathbf{g}_m$ parameters

Here we present our results about the $\mathbf{g}(\Phi_i^s, M_i^0)$ function [15,16] described in Sec. III B. The memory functions $M_i^0(q,t)$ are evaluated from the MD data for $\Phi_i^s(q,t)$ by Fourier transformation along the positive time axis. For completeness, also $T=800$ and 900 K data are included where the corresponding $\Phi_i^s(q,t)$ are extrapolated to longer times by use of an KWW approximation.

Figure 7 shows the thus deduced $M_i^0(q,t)$ for $q = 21.6$ nm$^{-1}$. Regarding their qualitative features, the obtained $M_i^0(q,t)$ are in full agreement with the results in Ref. [16] for the Ni$_{0.5}$Zr$_{0.5}$ system. A particular interesting detail is the fact that there exists a minimum in $M_i^0(q,t)$ for both species, Ni and Zr, at all investigated temperatures around a time of 0.1 ps. Below this time, $\Phi_i^s(q,t)$ reflects the vibrational dynamics of the atoms. Above this value, the escape from the local cages takes place in the melt and the $\beta$-regime dynamics are developed. Apparently, the minimum is related to this crossover.

By use of the calculated memory functions, we can evaluate the $\mathbf{g}(\Phi_i^s, M_i^0)$, Eq. (24). In Fig. 8 this quantity is presented versus the corresponding value of $\Phi_i^s(q,t)$ and denoted as $\mathbf{g}(\Phi_i^s)$. For all the investigated temperatures, $\mathbf{g}(\Phi_i^s)$ has a maximum $\mathbf{g}_m(q,T)$ at an intermediate value of $\Phi$. In
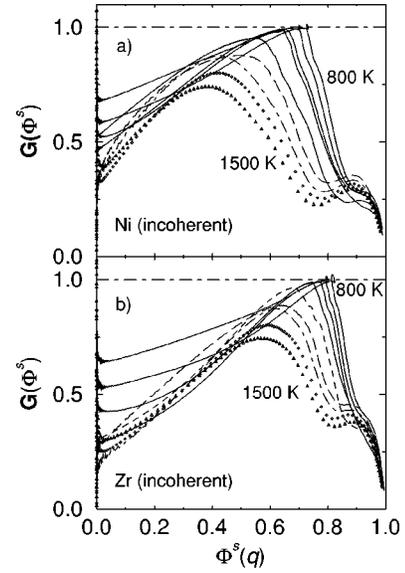


FIG. 8. MD simulation results for the characteristic function $\mathbf{g}(\Phi^s)$ as a function of $\Phi_i^s$ for $q = 21.6$ nm$^{-1}$; (a) Ni part and (b) Zr part.

the high temperature regime, the values of $\mathbf{g}_m(q,T)$ move with decreasing temperature towards the limiting value 1. This is, in particular, visible in Fig. 9 where we present $\mathbf{g}_m(q,T)$ as a function of temperature for both species, Ni and Zr, and wave vectors $q_8 = 19.2$ nm$^{-1}$ and $q_9 = 21.6$ nm$^{-1}$. At temperatures above 1000 K, the $\mathbf{g}_m$ values increase approximately linear towards 1 with decreasing temperatures. Below 1000 K, they remain close below the limiting value of 1, a behavior denoted in Refs. [15,16] as a
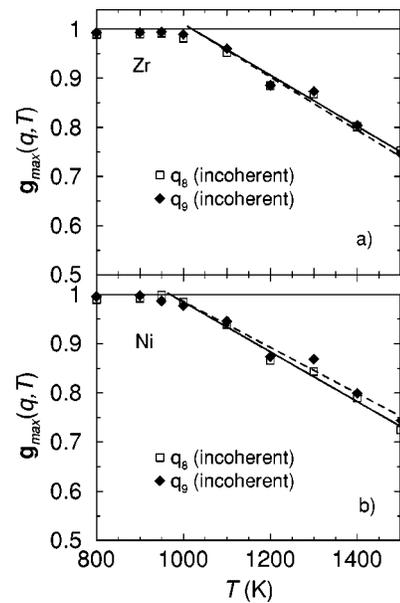


FIG. 9. MD simulation results of the temperature dependence of $\mathbf{g}_m(q,T)$ for $q_8 = 19.2$ nm$^{-1}$ (squares) and $q_9 = 21.6$ nm$^{-1}$ (diamonds). Linear fits to the $\mathbf{g}_m(q,T)$ are included by full and dashed lines (for $q_8 = 19.2$ nm$^{-1}$ and $q_9 = 21.6$ nm$^{-1}$, respectively); (a) Zr part with $T_c = 1020$ K and (b) Ni part with $T_c = 970$ K.
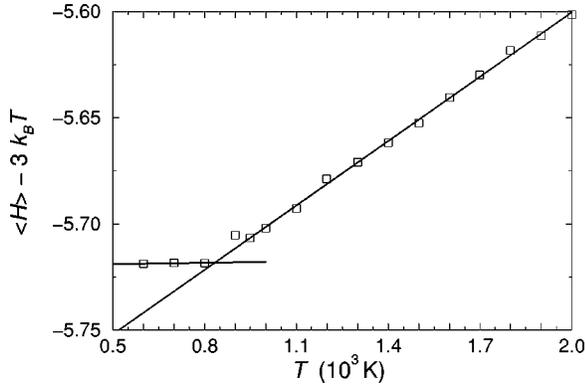
FIG. 10. MD simulation results on the enthalpy $H$ of the undercooled $Ni_{0.2}Zr_{0.8}$ melt and glass.



FIG. 11. Diffusion coefficients $D_i$ as a function of $1000/T$. Symbols are MD results for Ni (squares) and Zr (diamonds); the full line are power-law approximations for Ni and for Zr, respectively.

balancing on the borderline between the arrested and the nonarrested state due to thermally induced matter transport by diffusion in the arrested state at the present high temperatures.

Linear fit of the $\mathbf{g}_m$ values for Ni above 950 K and for Zr above 1000 K predicts a crossover temperature $T_c^*$ from liquid ($\mathbf{g}_m < 1$) to the quasiarrested ($\mathbf{g}_m = 1$) behavior around 970 K from the Ni data and around 1020 K from the Zr data. We here identify this crossover temperature with the value of $T_c$ as visible in the ergodic, liquid regime and estimate it by the mean value from the Ni and Zr subsystems, that means, by $T_c = 1000$ K.

While in Refs. [15,16] for the $Ni_{0.5}Zr_{0.5}$ melt a $T_c$ value of 1120 K was estimated from $\mathbf{g}_m(T)$, the value for the present composition is lower by about 120 K. A significant composition dependence of $T_c$ is expected according to the results of MD simulation for the closely related $Co_xZr_{1-x}$ system [48]. Over the whole $x$ range, $T_c$ was found to vary between 1170 and 650 K in $Co_xZr_{1-x}$, with $T_c(x=0.2) \simeq 800$ K. Regarding this, the present data for the $Ni_xZr_{1-x}$ system reflect a rather weak $T_c$ variation.

## D. Caloric glass temperature, diffusion coefficients, and $\alpha$-relaxation time

The present section provides additional results of our simulations aimed to enlighten the $T_c$ estimates of the previous section.

*Caloric glass temperature $T_G$.* First we consider the caloric glass temperature $T_G$ as observed, e.g., in the specific heat or, equivalently, by a change of slope in the enthalpy vs temperature dependence. For the rapid quench situation modeled by our simulations, $T_G$ depends strongly on the cooling rate. It indicates the temperature below which the system with decreasing temperature falls out of equilibrium as the relaxation time becomes too large compared with the cooling rate.

Figure 10 displays our simulation results. We present for a cooling rate of $10^{10}$ K/s the reduced enthalpy per atom, $\langle H \rangle - 3k_BT$, as a function of temperature. The subtracted term $3k_BT$ means the averaged thermal vibration energy of an atom and its subtraction makes more obvious the configuration dependent energy contributions [26]. Figure 10 clearly
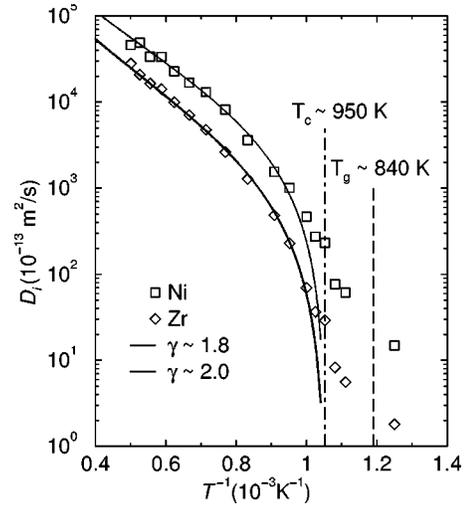
indicates a change of slope around a value of 840 K that we identify with $T_G$ for the applied cooling rate. Compared with the $T_c$ value from the $\mathbf{g}_m$ parameters, the $T_G$ obtained here is lower than $T_c$ by 160 K. Thus, for the present $Ni_{0.2}Zr_{0.8}$ composition, the temperature difference between $T_c$ and $T_G$ is larger than that for $Ni_{0.5}Zr_{0.5}$, $T_c - T_G \simeq 70$ K [15,16], although a lower cooling rate was used there. It is rather tempting to look for MD model systems with an extended temperature regime between $T_c$ and $T_G$ in order to study the dynamics in this region. At the present stage, however, we cannot give any indication for the mechanisms that determine the change of $T_c - T_G$ with composition at a fixed cooling rate.

*Diffusion coefficients.* From the simulated atomic motions in the computer experiments, the diffusion coefficients of the Ni and Zr species can be determined as the slope of the atomic mean square displacements in the asymptotic long-time limit

$$D_i(T) = \lim_{t \to \infty} \frac{(1/N_i) \sum_{\alpha=1}^{N_i} |\mathbf{r}_\alpha(t) - \mathbf{r}_\alpha(0)|^2}{6t}. \qquad (32)$$

Figure 11 shows the thus calculated diffusion coefficients of our $Ni_{0.2}Zr_{0.8}$ model for the temperature range between 800 and 2000 K. At temperatures above approximately 1250 K, the diffusion coefficients for both species run parallel to each other in the Arrhenius plot, indicating a fixed ratio $D_{Ni}/D_{Zr} \approx 2.5$ in this temperature regime. At lower temperatures, the Zr atoms have a lower mobility than the Ni atoms, yielding around 900 K a value of about 10 for $D_{Ni}/D_{Zr}$. That means, here the Ni atoms carry out a rather rapid motion within a relative immobile Zr matrix.

According to the idealized MCT, above $T_c$ the diffusion coefficients follow a critical power law

$$D_i(T) \sim |T - T_c|^\gamma \quad \text{for} \quad T > T_c \qquad (33)$$

with nonuniversal exponent $\gamma$ [47,44]. The upper and lower temperature of validity of this relation are not well known. While the idealized theory predicts a validity of the critical power law for an unspecified limited regime above $T_c$, the effects of transverse currents in the full MCT and thermally activated processes yield around and below $T_c$ a predominance of additional channels of matter transport beyond those described by this relation. Accordingly, this law is not expected to be fulfilled close to $T_c$ and far above $T_c$. For the mid-concentration system $Ni_{0.5}Zr_{0.5}$, the MD study [24] has shown that the critical law with $T_c$ from a $\mathbf{g}_m$ analysis holds rather well in the temperature range of about 100–900 K above $T_c$. Regarding this, in order to test the relation Eq. (33) and its usefulness for getting a raw estimate of $T_c$ for the present low-Ni-content system, we have adapted the critical power law by a least mean squares fit to the simulated diffusion data above $T_{min} = 1050$ K. As proposed in Ref. [48], the lower limit $T_{min}$ of the data included in the fit is taken from looking in the intermediate scattering function for aging effects on the time scale of the simulations. $T_{min}$ is introduced as the lower temperature limit for which no aging effects are detected. The results of the fit are presented in Fig. 11 by dashed lines. The fit leads to a critical temperature of 950 K. The parameters $\gamma$ turn out as 1.8 for the Ni subsystem and 2.0 for the Zr system.

Similar results for the temperature dependence of the diffusion coefficients have been found in MD simulations for other metallic-glass-forming systems, e.g., for $Ni_{0.5}Zr_{0.5}$ [24], for $Co_xZr_{1-x}$ [48], $Cu_{0.33}Zr_{0.67}$ [49], or $Ni_{0.81}B_{0.19}$ [50]. In all cases, like here, a break is observed in the Arrhenius slope. In the mentioned Zr systems, this break is related to a change of the atomic dynamics around $T_c$ whereas for $Ni_{0.81}B_{0.19}$ system it is ascribed to $T_G$. As in Ref. [50] $T_c$ and $T_G$ apparently fall together, there is no serious conflict between the observations.

A comment is necessary here concerning the comparison with experiments. Experimentally, around $T_G$ a break is observed in the Arrhenius slope in a number of investigations [51–54] while the vicinity of the presumed $T_c$ is not covered by the present diffusion studies of the metallic glasses and melts. According to our understanding, a break in the Arrhenius slope is expected around $T_c$ as it reflects the change of the mechanism of structural dynamics described by the MCT. In Refs. [51–53], the break around $T_G$ is ascribed to a change in frequency and phase space volume explored by the fluctuations when passing $T_G$. It depends significantly on the interplay between the time scale of the structural fluctuations and the hopping rate of the diffusing atoms, yielding that the break in the Arrhenius slope takes place at different temperatures for different diffusing species. Recent experiments [55] indicate that the break vanishes with further, more complete relaxation of the glassy state and that it thus, apparently, reflects a difference in the degree of structural relaxation of the system above and below $T_G$.

*$\alpha$-relaxation time*. The $\alpha$-relaxation time $\tau_\alpha(q,T)$ characterizes the time at which the final $\alpha$ decay of the scattering functions takes place. Suitable estimates of this time can be obtained by fitting a KWW law to the scattering functions at times beyond the $\beta$ regime. Values $\tau_\alpha(q,T)$ for $q_4$
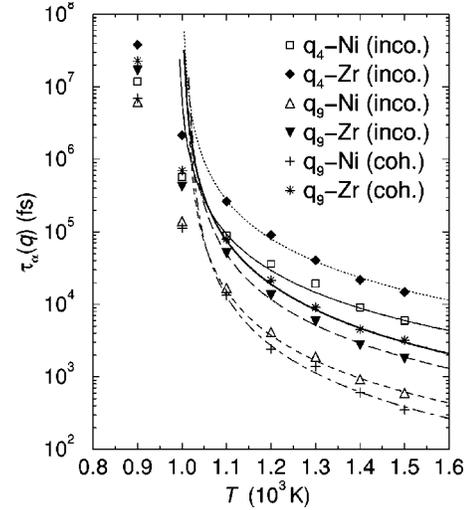


FIG. 12. $\alpha$-relaxation time $\tau_\alpha(q)$ as a function of $T(K)/1000$ for $q_4 = 9.6$ nm$^{-1}$ and $q_9 = 21.6$ nm$^{-1}$. The lines are the corresponding power-law fits. (see Table I for exponent parameter $\gamma$ and $T_c$).

$= 9.6$ nm$^{-1}$ and $q_9 = 21.6$ nm$^{-1}$ are presented in Fig. 12 for Ni and Zr, for the incoherent and partly for the coherent scattering.

According to the idealized MCT, the $\tau_\alpha(q,T)$ for temperatures above $T_c$ follow a critical power law

$$\tau_\alpha(q,T) \sim |T - T_c|^{-\gamma} \qquad (34)$$

also with nonuniversal parameter $\gamma$. Regarding the validity of this relationship, the same arguments hold as for Eq. (33) and estimations of $T_c$ from the relationship for $\tau_\alpha(q,T)$ are subjected to the same limitations as those from $D_i(T)$.

Having in mind these limitations, we present in Fig. 12 least squares fits of the critical power law to the obtained $\tau_\alpha(q,T)$ values for temperatures above $T_{min}$. The values of $T_c$ and of the $\gamma$ parameter determined in this way are given by Table I. The $T_c$ thus estimated varies between 990 and 1015 K and is slightly higher than from the diffusion coefficients, but in good agreement with the value from the $\mathbf{g}_m$ parameter. The $\gamma$ parameter for Ni and Zr varies between about 1.8 and 2.0. For temperatures below 1000 K, the $\tau_\alpha(q,T)$ values lie below the critical law and indicate that the structural correlations in this temperature regime decay by relaxation channels not included in the idealized MCT.

TABLE I. Critical temperature $T_c$ and parameters $\gamma$ from the $\alpha$-relaxation time.

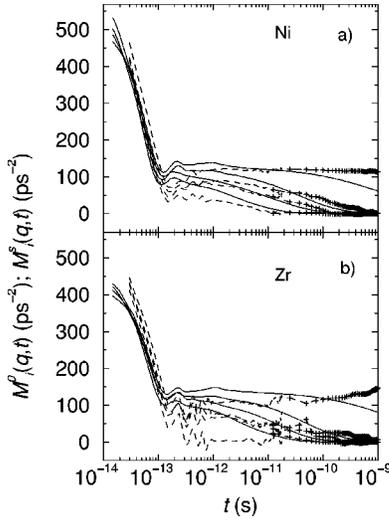| | Incoherent | | | | Coherent | | | |
|---|---|---|---|---|---|---|---|---|
| | Ni | | Zr | | Ni | | Zr | |
| $q$ values | $T_c$(K) | $\gamma$ | $T_c$(K) | $\gamma$ | $T_c$(K) | $\gamma$ | $T_c$(K) | $\gamma$ |
| $q = 9.2$ nm$^{-1}$ | 990 | 1.8 | 1000 | 1.8 | | | | |
| $q = 21.6$ nm$^{-1}$ | 1010 | 1.9 | 1010 | 1.9 | 1015 | 2.0 | 1000 | 2.0 |

FIG. 13. Comparison between $M_i^0(q,t)$ from MD simulations (full lines) and MCT results (dashed lines and symbols) for the memory function at $q=21.6$ nm$^{-1}$ and $T=900, 1000, 1100$, and 1200 K (from top to bottom); (a) Ni part and (b) Zr part.

### E. Memory function for the incoherent intermediate scattering function

Having evaluated in Sec. IV C the memory function $M_i^0(q,t)$ from the time evolution of the incoherent intermediate scattering function, it is tempting to compare this kernel with the prediction of the MCT. For comparison, we use for this kernel the MCT expression from the idealized theory that takes into account the density fluctuations and their coupling to the longitudinal currents in the ''one-loop'' approximation and is given by Eq. (8). The latter expression is augmented according to the proposal of Balucani and Zoppi [56] by adding explicitly to $M_i^s(q,t)$ a binary collision term $M_{B,i}^s(q,t)$ and replacing for compensation $F_i^s(q,t)$ with $F_i^s(q,t)-F_{0,i}^s(q,t)$, that means subtraction of the ballistic part $F_{0,i}^s(q,t)=\exp(-q^2t^2k_BT/2m_i)$. In order to include the effects of the attractive interaction potential between the atoms and the therefrom resulting vibrations as far as possible, we substitute the binary collision term $M_{B,i}^s(q,t)$ with the short time expression proposed by Balucani and Zoppi [56] with characteristic time $\tau_s(q)$ adapted to our simulations.

Figure 13 presents our results for $M_i^s(q,t)$ as obtained according to Eq. (8) with the above-mentioned amendments by use of the simulated partial structure factors and the simulated intermediate scattering functions. Included are in Fig. 13 the memory kernels $M_i^0(q,t)$ from inverting the time evolution of the incoherent intermediate scattering function as described in Sec. IV C. Figure 13(a) demonstrates that for Ni the magnitude of the memory kernel $M_i^0(q,t)$ in the time windows between $10^{-12}$ and $10^{-10}$ s is well reflected by the calculated $M_i^s(q,t)$ for the temperature around 1100 K and below. Figure 13(b) indicates that for Zr in the same time and temperature range the calculated $M_i^s(q,t)$ seem by about 30–40 % below the estimated $M_i^0(q,t)$. Deviations are found at 900 K in the long time behavior. There the calulcated $M_i^s(q,t)$ is found above the estimated $M_i^0(q,t)$, perhaps due

to diffusion effects missing in Eq. (8). Significant deviations are especially seen in the 1200 K curves. Here the calculated $M_i^s(q,t)$ show a rather rapid decay, basically induced by interference effects in the evaluation of the momentum integrations of Eq. (8). It remains an open question whether for this temperature an improved agreement between calculated $M_i^s(q,t)$ and estimated $M_i^0(q,t)$ can be obtained by inclusion of the coupling to transverse currents in the memory kernel formula as provided, e.g., by Gudowski *et al.* [57].

### V. CONCLUSION

The present contribution reports results from MD simulations of a Ni$_{0.2}$Zr$_{0.8}$ computer model. The model is based on the electron theoretical description of the interatomic potentials for transition metal alloys by Hausleitner and Hafner [31]. There are no parameters in the model adapted to the experiments. Comparison of the calculated structure factors with experiments [20] indicates that the model is able to reproduce sufficiently well the steric relations and chemical order in the system, as far as visible in the structure factors.

There is close agreement between the $T_c$ values estimated from the dynamics in the undercooled melt when approaching $T_c$ from the high temperature side. The values are $T_c \approx 970$–1020 K from the $\mathbf{g}_m$ parameters, $T_c \approx 990$–1015 K from the $\alpha$-relaxation time, and $T_c \approx 950$ K from the diffusion coefficients. As discussed in Ref. [48], the $T_c$ estimates from the diffusion coefficients seem to depend on the upper limit of the temperature region taken into account in the fit, where an increase of the upper limit increases the estimated $T_c$. Accordingly, there is evidence that the present value of 950 K may underestimate the true $T_c$ by about 10–50 K, as it is based on an upper limit of 2000 K only. Taking this into account, the present estimates from the melt seem to lead to a $T_c$ value around 1000 K.

The $T_c$ from the nonergodicity parameters describe the approach of the system towards $T_c$ from the low temperature side. They predict a $T_c$ value of 1100 K. This value is outside the range of $T_c$ estimates from the so-called ergodic melt. There is, however, fair agreement between the data, and our results reconfirm the finding from the soft spheres model [18] of an agreement within 10% between the different $T_c$ estimates.

Further, we compared the memory kernels $M_i^s(q,t)$ evaluated from the MCT formula with the kernels $M_i^0(q,t)$ from inverting the time evolution of the intermediate scattering functions. The comparison shows encouraging agreement at 900–1100 K while significant deviations are found at 1200 K. As already mentioned, it is an open question whether for this temperature an improved agreement between calculated $M_i^s(q,t)$ and estimated $M_i^0(q,t)$ can be obtained by inclusion of the coupling to transverse currents in the memory kernel formula.

### ACKNOWLEDGMENT

[1] J. Jäckle, Rep. Prog. Phys. **49**, 171 (1986).

[2] W. Götze and L. Sjögren, Rep. Prog. Phys. **55**, 241 (1992).

[3] W. Götze, J. Phys.: Condens. Matter **11**, A1 (1999).

[4] H.Z. Cummins, G. Li, Z.H. Hwang, G.Q. Shen, W.M. Du, J. Hernandes, and N.J. Tao, Z. Phys. B: Condens. Matter **103**, 501 (1997).

[5] L.P. Kadanoff and J. Swift, Phys. Rev. **166**, 89 (1968).

[6] K. Kawasaki, Phys. Rev. **150**, 1 (1966); Ann. Phys. (N.Y.) **61**, 1 (1970).

[7] M.H. Ernst and J.R. Dorfman, J. Stat. Phys. **12**, 311 (1975).

[8] U. Bengtzelius, W. Götze, and A. Sjölander, J. Phys. C **17**, 5915 (1984).

[9] E. Leutheusser, Phys. Rev. A **29**, 2765 (1984).

[10] P.S. Das and G.F. Mazenko, Phys. Rev. A **34**, 2265 (1986).

[11] L. Sjögren, Z. Phys. B: Condens. Matter **79**, 5 (1990).

[12] T. Gleim and W. Kob, Eur. Phys. J. B **13**, 83 (2000).

[13] A. Meyer, R. Busch, and H. Schober, Phys. Rev. Lett. **83**, 5027 (1999); A. Meyer, J. Wuttke, W. Petry, O.G. Randl, and H. Schober, *ibid.* **80**, 4454 (1998).

[14] H.Z. Cummins, J. Phys.: Condens. Matter **11**, A95 (1999).

[15] H. Teichler, Phys. Rev. Lett. **76**, 62 (1996).

[16] H. Teichler, Phys. Rev. E **53**, 4287 (1996).

[17] J.L. Barrat and A. Latz, J. Phys.: Condens. Matter **2**, 4289 (1990).

[18] M. Fuchs, Dr. rer. nat. thesis, TU-Muenchen, 1993; M. Fuchs and A. Latz, Physica A **201**, 1 (1993).

[19] M. Nauroth and W. Kob, Phys. Rev. E **55**, 657 (1997).

[20] M. Kuschke, Dr. rer. nat. thesis, Universität Stuttgart, 1991.

[21] Yan Yu, W.B. Muir, and Z. Altounian, Phys. Rev. B **50**, 9098 (1994).

[22] B. Böddeker, Dr. rer. nat. thesis, Universität Göttingen, 1999; B. Böddeker and H. Teichler, Phys. Rev. E **59**, 1948 (1999).

[23] H. Teichler, Phys. Status Solidi B **172**, 325 (1992).

[24] H. Teichler, Defect Diffus. Forum **143-147**, 717 (1997).

[25] H. Teichler, in *Simulationstechniken in der Materialwissenschaft*, edited by P. Klimanek and M. Seefeldt (TU Bergakadamie, Freiberg, 1999).

[26] H. Teichler, Phys. Rev. B **59**, 8473 (1999).

[27] T. Aihara, K. Aoki, and T. Masumoto, Mater. Trans., JIM **36**, 399 (1995).

[28] T. Aihara, Y. Kawazoe, and T. Masumoto, Sci. Rep. Res. Inst. Tohoku Univ. A **41**, 1 (1995).

[29] T. Aihara and T. Masumoto, J. Phys.: Condens. Matter **7**, 1525 (1995).

[30] T. Aihara, Y. Kawazoe, and T. Masumoto, Sci. Rep. Res. Inst. Tohoku Univ. A **42**, 57 (1996).

[31] Ch. Hausleitner and Hafner, Phys. Rev. B **45**, 128 (1992).

[32] A. B. Mutiara, Dr. rer. nat. thesis, Universität Göttingen, 2000.

[33] W. Götze, Z. Phys. B: Condens. Matter **60**, 195 (1985).

[34] J. Bosse and J.S. Thakur, Phys. Rev. Lett. **59**, 998 (1987).

[35] B. Bernu, J.-P. Hansen, G. Pastore, and Y. Hiwatari, Phys. Rev. A **36**, 4891 (1987); **38**, 454 (1988).

[36] W. Götze and L. Sjörgen, J. Phys. C **21**, 3407 (1988).

[37] W. Götze and R. Haussmann, Z. Phys. B: Condens. Matter **72**, 403 (1988).

[38] C. Lanczos, J. Res. Natl. Bur. Stand. **45**, 255 (1950).

[39] R. Zwanzig, J. Chem. Phys. **33**, 1338 (1960); H. Mori, Prog. Theor. Phys. **33**, 423 (1965).

[40] J. P. Hansen and I. R. McDonald, *Theory of Simple Liquids*, 2nd ed. (Academic Press, London, 1986).

[41] W. Kob and H.C. Andersen, Phys. Rev. E **52**, 4134 (1995).

[42] T.E. Faber and J.M. Ziman, Philos. Mag. **11**, 153 (1965).

[43] Y. Waseda, *The Structure of Non-Crystalline Materials* (McGraw-Hill, New York, 1980).

[44] J.-P. Hansen and S. Yip, Transp. Theory Stat. Phys. **24**, 1149 (1995).

[45] W. Kob and J.L. Barrat, Physica A **263**, 1 (1999); Phys. Rev. Lett. **78**, 4581 (1997).

[46] W. H. Press, B. P. Flannery, S. A. Teukolsky, and W. T. Vetterling, *Numerical Recipes*, 2nd edition (Cambridge University Press, New York, 1992).

[47] W. Kob and H.C. Andersen, Phys. Rev. E **51**, 4626 (1995).

[48] U. Rössler and H. Teichler, Phys. Rev. B **61**, 394 (2000).

[49] C. Gaukel, Dr. rer. nat. thesis, TU-Aachen, 1998.

[50] L. D. van Ee, Dr. thesis, TU-Delft, 1998.

[51] K. Knorr, Dr. rer. nat. thesis, Universität Münster, 2000.

[52] U. Geyer, S. Schneider, W.L. Johnson, Y. Qiu, T.A. Tombrello, and M.-P. Macht, Phys. Rev. Lett. **75**, 2364 (1995).

[53] P. Filietz, M. Macht, V. Naundorf, and G. Frohberg, J. Non-Cryst. Solids **250**, 674 (1999).

[54] X.-P. Tang, U. Geyer, R. Busch, W.L. Johnson, and Yue Wu, Nature (London) **402**, 160 (1999).

[55] Th. Zumkley, V. Naundorf, M.-P. Macht, and G. Frohberg, Scr. Metall. Mater. (to be published).

[56] U. Balucani and M. Zoppi, *Dynamics of the Liquid State* (Oxford Science Publications, Oxford, 1994).

[57] W. Gudowski, M. Dzugutov, and K.E. Larsson, Phys. Rev. E **47**, 1693 (1993); J. Non-Cryst. Solids **156-158**, 125 (1993).